

Precise high resistance comparison between the NMIJ traveling dual source bridge and the NIST adapted Wheatstone bridge

T Oe^{1,*}, S Payagala², A R Panna², S Takada¹, N-H Kaneko¹ and D G Jarrett^{2,*}

¹ National Metrology Institute of Japan (NMIJ), Advanced Industrial Science and Technology (AIST), Tsukuba, 305-8563, Japan

² National Institute of Standards and Technology (NIST), Gaithersburg, MD 20899, United States of America

E-mail: t.oe@aist.go.jp and dean.jarrett@nist.gov

Received 2 June 2022, revised 25 September 2022

Accepted for publication 30 September 2022

Published 28 October 2022



CrossMark

Abstract

A precise high resistance comparison was performed between the traveling dual source bridge developed by the National Metrology Institute of Japan (NMIJ) and the adapted Wheatstone bridge of the National Institute of Standards and Technology (NIST) from 10 M Ω to 100 T Ω at NIST. The NMIJ traveling bridge was shipped to NIST Gaithersburg and was installed right next to the NIST bridge and these bridges alternately measured the resistance ratio of the high resistance standards, without moving the location of the resistors inside the temperature controlled air-bath. Having the bridges and resistance standards in the same location for the comparison decreased the transportation and temperature coefficient effects on the resistance standards, contributing to the excellent agreement of the measured values. The NMIJ traveling bridge used an 8.5-digit digital multimeter and a relay switch box to determine a resistance ratio by measuring the ratio of the voltages applied to the resistors. The comparison was started from 10 M Ω based on the same 1 M Ω standard resistor calibrated using a NIST two-terminal cryogenic current comparator bridge, and standard resistors from 10 M Ω to 100 T Ω were calibrated by repeating 10 : 1 scaling measurements with both systems. Excellent agreement was obtained within the uncertainty of all resistance ranges and the difference between both systems was less than 1 $\mu\Omega \Omega^{-1}$ up to 1 T Ω and the degrees of equivalence for 10 T Ω and 100 T Ω were less than 6 $\mu\Omega \Omega^{-1}$.

Keywords: high resistance measurement, small current measurement, DC resistance standards, international comparison, adaptive Wheatstone bridge, traveling dual source bridge

(Some figures may appear in colour only in the online journal)

1. Introduction

High resistance standards have an important role in small current measurements in development of insulation materials, low-dose-rate radiation dosimetry, single electron transport,

and purity of materials. Precise high voltage measurement and generation of stable electrical power also require a high resistance standard as a key element. To compare the high resistance measurement capabilities, the National Metrology Institute of Japan (NMIJ) and the National Institute of Standards and Technology (NIST) have performed high resistance measurement comparisons for several years, which yielded

* Authors to whom any correspondence should be addressed.

excellent agreement within the expanded uncertainties ($k = 2$) for 10 T Ω and 100 T Ω [1]. International comparison is usually performed using traveling resistors and the stability of these resistors is crucial to evaluate the equivalence of the measurements [2–4]. In this comparison, the NMIJ traveling dual source bridge (DSB) was sent to NIST as a traveling standard instrument to decrease the influence of the instability of the resistors due to transport, minimize resistor impact on the comparison results and perform high resistance measurement comparisons more precisely. Minimizing resistor drift and environmental effects provides an ideal condition to evaluate the equivalence of the two systems of the NIST and NMIJ.

Recent digital multimeters have good voltage measurement linearity better than 10^{-7} or less [5–8]. The NMIJ traveling DSB measures the voltage ratio applied to standard resistors using a 8.5-digit digital multimeter, as shown in figure 1, to derive the resistance ratio. It is expected that the linearity of a multimeter is more stable than the resistance value of the traveling resistors and the calibrated output voltage value of voltage sources, so this bridge circuit configuration could be suitable as a traveling standard.

The NMIJ traveling DSB was installed next to the third generation of the NIST adapted Wheatstone bridge (AWB) and resistance standards from 10 M Ω to 100 T Ω [9] were alternately measured without moving the resistors, located inside a temperature controlled air bath [10]. The NIST AWB uses well characterized voltage sources to apply voltage corrections to derive the correct resistance ratio. Both bridges are based on the method of the automated high resistance bridge proposed by Henderson [11] but use entirely different hardware. The bridges are configured with programmable voltage sources in the main ratio arms. To clearly distinguish the AIST and NIST bridges in this manuscript, we refer to the AIST bridge as a DSB and the NIST bridge as an AWB.

The high resistance comparison was performed starting with a stable 1 M Ω standard resistor calibrated precisely using the two-terminal cryogenic current comparator bridge at NIST [12, 13]. Many of the resistors used in this comparison were fabricated at NIST [9] for improved stability, low voltage dependence, and low temperature dependence. The other resistors were commercially available, using similar fabrication techniques. All resistors were adequately maintained in the NIST as reference standards. The comparison was performed with the applied voltage of 100 V up to 1 T Ω , and 200 V was used for 10 T Ω and 100 T Ω . This relatively low applied voltage was due to the acceptable voltage of the homemade switch box of the NMIJ traveling bridge but we obtained good comparison results even with such a low applied voltage. This regularly calibrated and well-characterized 1 M Ω resistor was used in both high resistance measurement systems as the initial reference. The comparison built up to 100 T Ω by repeating 10:1 ratio measurements, and these calibrated values, by both systems, agreed well to within their uncertainties at each nominal resistance value from 10 M Ω to 100 T Ω [14].

In this article, the details of both bridges and their measurement algorithms are described and the comparison results

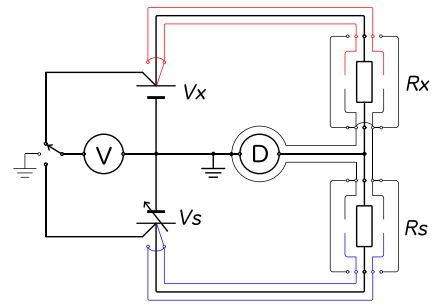


Figure 1. Circuit diagram of the NMIJ traveling DSB. The resistance ratio, R_x/R_s , is determined from the measured voltages of V_x and V_s using the digital multimeter V . The NIST AWB circuit diagram is the same except that it does not have a multimeter V .

from 10 M Ω to 100 T Ω are shown between the NMIJ traveling DSB and the NIST AWB. A comparison between the NMIJ traveling DSB and the NMIJ modified Wheatstone bridge, which is regularly used for calibrations for clients in Japan [15] will be performed in the future.

2. Measurement system

2.1. NMIJ traveling DSB

The circuit diagram of the NMIJ traveling DSB is shown in figure 1. The system is composed of two 6.5-digit voltage sources (ADCMT 6166)³, a current detector (Femto DDPCA-300 and Keithley DMM7510), a digital multimeter (Hewlett Packard 3458A) to measure the source voltages, and a homemade switch box with latching relays. The latching relays are controlled by a universal serial bus (USB) input/output device with LabVIEW software. All equipment is operated by a laptop personal computer connected through a USB isolator to prevent ground loop and noise problems.

The error current flowing through the current detector was converted to voltage using a transimpedance amplifier (Femto DDPCA-300) [16, 17] and the output voltage was measured using a 7.5 digit digital multimeter (Keithley DMM7510) in the entire resistance range of 10 M Ω to 100 T Ω instead of using a voltmeter as a detector [18]. The low terminal of the DMM7510 and the chassis of all equipment were connected to a common ground. An active guarding circuit was implemented by applying V_x and V_s to the cable shields and the split guard of the resistance boxes as shown in figure 1 to shorten the settling time [19, 20].

The measurement sequence of the NMIJ traveling DSB is shown below and the typical output voltage of the detector D

³ Certain commercial equipment, instruments, or materials are identified in this paper to foster understanding. Such identification does not imply recommendation or endorsement by the National Institute of Standards and Technology, nor does it imply that the materials or equipment identified are necessarily the best available for the purpose.

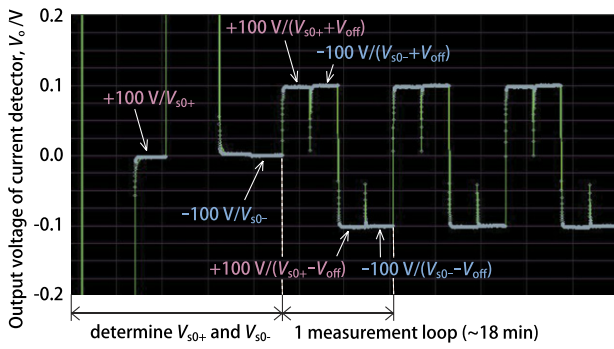


Figure 2. Output voltage of the current detector D (10^{11} V A^{-1}) as a function of time during $10 \text{ G}\Omega/1 \text{ G}\Omega$ measurement of the NMIJ traveling DSB.

as a function of time is shown in figure 2. At the beginning part of the measurement, the bridge software determined V_{s0+} and V_{s0-} by getting bridge balance roughly by adjusting V_s to achieve zero readings on the detector D for positive and negative V_x , respectively as shown in figure 2.

- (a) Apply nominal ratio voltages (e.g. $V_x/V_s = +100 \text{ V} / -10 \text{ V}$) and the voltage V_s is adjusted so that the current detector D shows zero and determine the bridge balance voltage (V_{s0+}).
- (b) Repeat the same process for reversed polarity ($-100 \text{ V} / +10 \text{ V}$) and determine V_{s0-} . Then the main measurement sequence as below is repeated for the specified number of times.
- (c) Apply the voltages of $V_x/V_s = +100 \text{ V} / (V_{s0+} + V_{\text{off}})$, where the V_{off} is a specified voltage offset, and measure the current through the detector D . The voltage ratio of V_x/V_s was measured using the digital multimeter V (3458A) before and after the current measurement. The typical value of the V_{off} is from 0.01 mV ($1 \mu\text{V V}^{-1}$ of 10 V) to 1 mV ($100 \mu\text{V V}^{-1}$ of 10 V).
- (d) (c) is repeated with the applied voltages of $V_x/V_s = -100 \text{ V} / (V_{s0-} + V_{\text{off}})$, $+100 \text{ V} / (V_{s0+} - V_{\text{off}})$, and $-100 \text{ V} / (V_{s0-} - V_{\text{off}})$ as shown in figure 2.
- (e) (c) and (d) are repeated for specified number of loops, typically 12.

The output voltage of V_x was evaluated in advance and the set value was determined for both polarities so that the absolute value was exactly 100 V . For the measurement of the voltages V_x and V_s , the same voltage range of the 3458A was used to achieve an accurate voltage ratio. The 3458A input is connected to the ground during the current measurement and it is connected to V_x or V_s only during the voltage measurement. The voltage ratio measurement was performed before and after the current measurement to cancel the effect of the drift of the actual applied voltage.

Since the system measures the voltage ratio of the applied voltages and the current flowing through the current detector after getting the balance for each polarity, the measurement time is longer than the NIST AWB system which only measures the current.

2.2. NIST AWB

The NIST AWB uses two Fluke 57X0A calibrators as the stable voltage sources, and a Keithley 6430A as a current detector [21–24]. The output voltages of the 57X0As are calibrated in advance using a measurements International 8000A/8001A automated Cutkosky binary voltage divider [25, 26]. The voltage corrections are applied during the measurement to V_x and V_s . Two versions of the control software were available (LabVIEW and Visual Basic) which showed the same results within the uncertainty in the preliminary test for some particular range from $10 \text{ M}\Omega$ to $10 \text{ G}\Omega$. The LabVIEW program adopts the ‘true zero’ algorithm [21] to suppress the influence of the residual offset current and to enable the measurement of the resistors with delta-wye configuration [27, 28], and need a longer measurement time than the Visual Basic program, which was used for the comparison. The detailed measurement algorithm is shown below:

- (a) The applied voltage to get the bridge balance (V_{s0+} and V_{s0-}) is calculated from the predicted value of the R_s and R_x using the historical data. If historical data is not available, nominal voltages are initially applied.
- (b) $V_x/V_s = +100 \text{ V} / (V_{s0+} + V_{\text{off}})$ is applied and the detector current is measured using the 6430A. Here, the V_{off} is the specified voltage offset and it is typical value is $5000 \mu\text{V V}^{-1}$.
- (c) (b) is repeated for $V_x/V_s = -100 \text{ V} / (V_{s0-} + V_{\text{off}})$, $+100 \text{ V} / (V_{s0+} - V_{\text{off}})$, and $-100 \text{ V} / (V_{s0-} - V_{\text{off}})$.
- (d) (b) and (c) are repeated for the specified number of loops.

The measurement program of the NMIJ traveling DSB was modified to adapt the same algorithm as that of the NIST Visual Basic program, so both systems use similar algorithms but were independently written. The NIST AWB and the NMIJ DSB initially apply approximate voltages calculated from the historical data of the resistance value of the R_s and R_x , then precisely adjust the applied voltage (V_{s0+} and V_{s0-}) to minimize the current flowing through the detector.

3. Uncertainty estimation

3.1. Uncertainty of the NMIJ traveling DSB

The NMIJ traveling DSB determines the resistance ratio R_x/R_s by measuring the voltage ratio V_x/V_s using the 3458A digital multimeter and the uncertainty of this voltage measurement is the main component of the measurement uncertainty in the lower range of high resistance. In the range of $1 \text{ T}\Omega$ and above, the resolution of the current detector becomes the major uncertainty component. Table 1 summarizes the measurement uncertainty of the NMIJ bridge in the comparison. In the following subsections, some uncertainty components are discussed.

3.1.1. Voltage ratio measurement. The uncertainty of the measured voltage ratio of $\pm 100 \text{ V} / \mp 10 \text{ V}$ using the same 100 V range can be calculated as $2.1 \mu\text{V V}^{-1}$ ($k = 2$) using the manufacturer’s specification values [29]. To assume the

Table 1. Measurement uncertainty of the NMIJ traveling DSB from 10 MΩ to 100 TΩ in this comparison.

R_x nominal	10 MΩ	100 MΩ	1 GΩ	10 GΩ	100 GΩ	1 TΩ	10 TΩ	100 TΩ
R_s uncertainty ($\mu\Omega\Omega^{-1}$)	0.10	0.44	0.62	0.76	0.88	1.03	3.11	23.4
Measured voltage ratio error ($\mu\Omega\Omega^{-1}$)	0.37	0.37	0.37	0.37	0.37	0.37	0.37	0.37
Detector resolution ($\mu\Omega\Omega^{-1}$)	0.035	0.035	0.040	0.07	0.29	2.9	23.1	231
Source instability ($\mu\Omega\Omega^{-1}$)	0.17	0.16	0.16	0.16	0.16	0.16	0.16	0.16
R_s voltage coefficient ($\mu\Omega\Omega^{-1}$)	0.1	0.2	0.2	0.2	0.2	0.3	1.7	2.9
Wiring resistance ($\mu\Omega\Omega^{-1}$)	0.12	0.01	0.001	—	—	—	—	—
Type A ($\mu\Omega\Omega^{-1}$)	0.01	0.01	0.04	0.06	0.11	0.11	0.28	29
Combined uncertainty ($\mu\Omega\Omega^{-1}$)	0.44	0.62	0.76	0.88	1.0	3.1	23.4	234
Expanded uncertainty ($k = 2$) ($\mu\Omega\Omega^{-1}$)	0.87	1.2	1.5	1.8	2.0	6.2	47	468

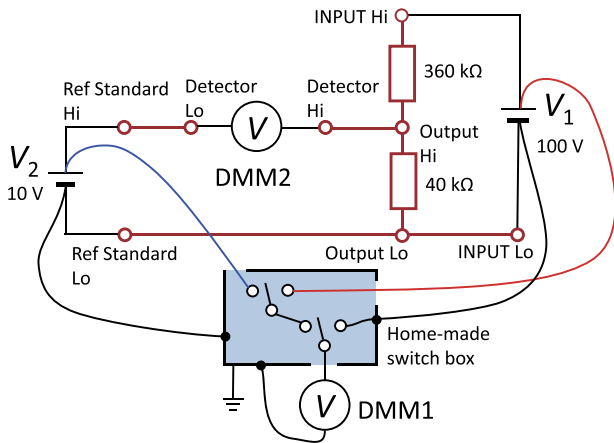


Figure 3. Circuit configuration for the calibration of the 3458A digital multimeter using a 10 : 1 reference voltage divider.

real uncertainty of the measured voltage ratio, we measured the calibrated voltages from Fluke 57X0A calibrator using the 3458A multimeter. The output voltages from the 57X0A calibrator were calibrated using a commercial binary voltage divider and the measured voltage ratio using 3458A agreed to the calibrated voltage ratio value within $0.2\ \mu\text{V}\ \text{V}^{-1}$.

To confirm the result, another calibration was performed using a Fluke 752A reference voltage divider. Figure 3 shows the circuit diagram of the calibration of the measured voltage ratio by the 3458A using a reference voltage divider. The ratio of the divider was adjusted in advance and the output of the voltage source V_2 was adjusted so that the digital multimeter DMM2 showed the lowest voltage and this measured residual voltage was also used for the calculation. Then the digital multimeter DMM1 measured the two voltage values and compared them to the earlier results, which agreed to within $0.6\ \mu\text{V}\ \text{V}^{-1}$.

Figure 4 shows the measured Allan deviation [30] of the measured 10 V using the 100 V range of the 3458A. The red dashed line in the graph shows the eye guide of $1/\sqrt{\tau}$ where τ is the measurement time. In this comparison, since the NMIJ system measured $\pm 100\ \text{V}$ and $\mp 10\ \text{V}$ with 60 points, each with ten power line cycles setting for each polarity, the voltage resolution was better than $0.2\ \mu\text{V}\ \text{V}^{-1}$.

We combined these values as the uncertainty of the voltage ratio measurement and it was $0.37\ \mu\text{V}\ \text{V}^{-1}$.

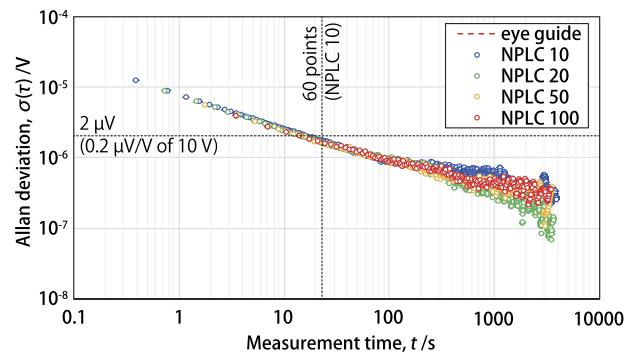


Figure 4. Allan deviation of the measured 10 V using the 100 V range of the 3458A.

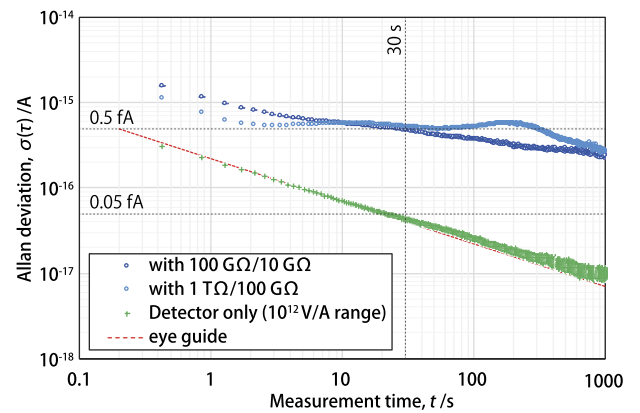


Figure 5. Allan deviation of the current detector, DDPCA-300, for the NMIJ traveling DSB.

3.1.2. Relay box. A home-made relay box, as shown in figure 3 composed of a set of latching relays was used to switch the voltages, V_x and V_s , at the input of the 3458A multimeter. The measured resistance of the relay box with wires and connectors was less than $1\ \Omega$, and is negligible compared to the input resistance of the 3458A. The fluctuation of the thermal electromotive force (EMF) also affects the measured voltage ratio. It was measured using the 3458A by connecting the inner pin to the shield box at its input. The measured thermal EMFs were a few microvolts and they were stable within $0.15\ \mu\text{V}$. As a result of calculating the effect on the actual measurement, it was less than $0.01\ \mu\Omega\ \Omega^{-1}$.

Table 2. Measurement uncertainty of the NIST AWB from 10 M Ω to 100 T Ω in this comparison.

R_x nominal	10 M Ω	100 M Ω	1 G Ω	10 G Ω	100 G Ω	1 T Ω	10 T Ω	100 T Ω
R_s uncertainty ($\mu\Omega\Omega^{-1}$)	0.10	0.21	0.30	0.38	0.45	0.56	0.83	3.23
Detector resolution ($\mu\Omega\Omega^{-1}$)	0.05	0.05	0.06	0.12	0.12	0.46	1.15	17.3
Voltage correction ($\mu\Omega\Omega^{-1}$)	0.12	0.12	0.12	0.12	0.12	0.12	0.12	0.12
R_s voltage coefficient ($\mu\Omega\Omega^{-1}$)	0.06	0.17	0.17	0.17	0.17	0.29	1.7	2.9
Wiring resistance ($\mu\Omega\Omega^{-1}$)	0.12	0.01	0.001	—	—	—	—	—
Type A ($\mu\Omega\Omega^{-1}$)	0.02	0.02	0.08	0.07	0.23	0.25	2.3	47.0
Combined uncertainty ($\mu\Omega\Omega^{-1}$)	0.21	0.30	0.38	0.45	0.56	0.83	3.23	50.2
Expanded uncertainty ($k = 2$) ($\mu\Omega\Omega^{-1}$)	0.42	0.60	0.76	0.90	1.1	1.7	6.5	101

3.1.3. Current detector. Figure 5 shows the Allan deviation of the current detector, DDPCA-300, for the NMIJ traveling DSB. The plus-sign marker show the measured Allan deviation of the detector without any connection at the 10^{12} V A $^{-1}$ range. The red dotted line shows $1/\sqrt{\tau}$ as an eye guide, where τ is the measurement time. According to the datasheet of a DDPCA-300 [16, 17], the spectral input noise current density is 1.3 fA $\sqrt{\text{Hz}^{-1}}$ for the 10^{10} and 10^{11} V A $^{-1}$ range and 0.2 fA $\sqrt{\text{Hz}^{-1}}$ for the 10^{12} and 10^{13} V A $^{-1}$ range, respectively, and similar results were obtained as shown in the figure. Two blue plots show the measured Allan deviation of the detector with the DSB and resistors with 100 G Ω /10 G Ω and 1 T Ω /100 G Ω . During this measurement, the voltage sources, V_x and V_s , output 0 V. Due to the noise from the cables, high resistance standards, and voltage sources, the current resolution of the detector strongly deteriorated in this situation.

The NMIJ DSB measures the current flowing through the detector after getting the balance for approximately 30 s for each polarity, then the current resolution for the 100 G Ω /10 G Ω and 1 T Ω /100 G Ω measurements can be assumed about 0.5 fA from the graph. During the 1 T Ω /100 G Ω measurement, 100 V was applied to the 1 T Ω resistor and the current flowing through the resistor was 100 pA. The 0.5 fA is $5/\sqrt{3} \simeq 2.9 \mu\Omega\Omega^{-1}$ of the 100 pA, leading to $5/\sqrt{3} \simeq 2.9 \mu\Omega\Omega^{-1}$ as the standard uncertainty due to the detector resolution for this resistance range with this applied voltage. The NMIJ DSB used the 10^{10} V A $^{-1}$ range for 10 M Ω and 100 M Ω measurements, the 10^{11} V A $^{-1}$ range for 1 G Ω and 10 G Ω measurements, the 10^{12} V A $^{-1}$ range for 100 G Ω and 1 T Ω measurements, and the 10^{13} V A $^{-1}$ range for 10 T Ω and 100 T Ω measurements, respectively. The uncertainty due to the current resolution for all resistance ranges was evaluated in a similar way.

3.1.4. Voltage sources. The internal resistance and the drift of the output voltage of the two voltage sources can cause an error. The internal resistance of the 6166 voltage sources are less than 100 m Ω according to the manufacturer's specifications. The smallest resistance connected to the right arm of the bridge is 1 M Ω and the internal resistance of 100 m Ω is $0.1 \mu\Omega\Omega^{-1}$ of it. In order to confirm the influence of the internal resistance of the voltage sources, the voltage ratios were measured with and without $R_x/R_s = 10 \text{ M}\Omega/1 \text{ M}\Omega$ resistors

after getting the bridge balance with the resistors. The measured voltage ratios with and without resistors agreed within $0.1 \mu\text{V V}^{-1}$ and 100 m Ω is used as the internal resistance of the sources to calculate the uncertainty.

The drift of the output voltages also affects the measured result. Since the voltage and current measurements after balance in the main measurement took about a minute for each polarity, we briefly evaluated the stability of the output voltage of the voltage sources for a minute and as a consequence, we estimate that it was stable within $0.2 \mu\text{V V}^{-1}$.

The uncertainty due to the instability of the voltage sources was considered about $0.16 \mu\text{V V}^{-1}$ since there were two voltage sources and the uncertainties due to the internal resistance of the sources were also taken into account according to the R_x and R_s .

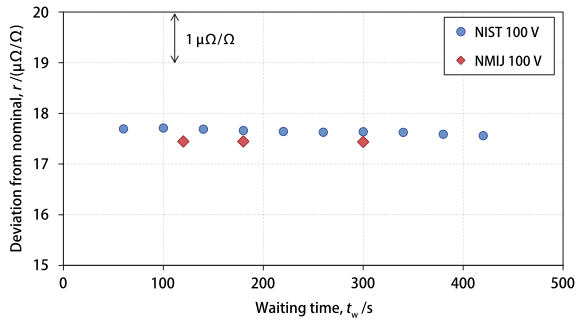
3.1.5. Other uncertainty sources. Wiring resistances between the resistors and the voltage sources affect the balancing voltages and these were approximately 200 m Ω . It is one of the main uncertainty components for 10 M Ω measurement but it can be negligible over 100 M Ω .

Voltage coefficient of R_s was evaluated based on the measurement results with different applied voltages and the uncertainty of the corrected R_s value was considered. The measured voltage dependence of the resistors will be shown in figure 7 and will be reported in section 4.

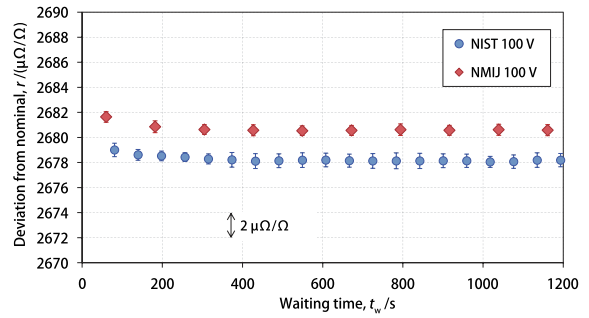
Type A uncertainties were calculated from the actual measurement data to be shown later.

3.2. Uncertainty of the NIST adaptive Wheatstone bridge

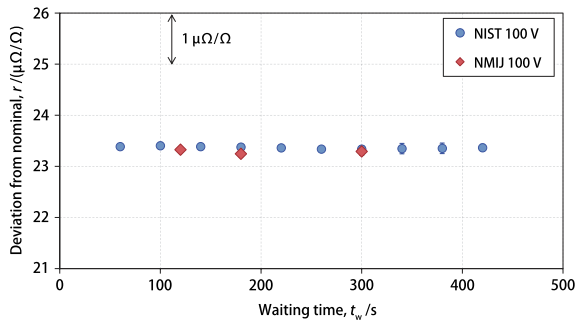
In the same manner as the NMIJ traveling DSB, the measurement uncertainty of the NIST AWB was calculated as shown in table 2. The NIST system uses two voltage sources calibrated in advance using a commercial Cutkosky divider with a Zener voltage standard and the output voltages were corrected during the measurement. The uncertainties of these voltage corrections were considered and are shown in table 2. The NIST AWB uses a Keithley 6430 as the current detector. The same procedure as used for the AIST bridge was applied to the NIST bridge to evaluate the detector resolution as described in section 3.1.3. The detector resolution was evaluated for the lowest range, 1 pA, and auto range, which sets the range to 100 pA for the lowest measured currents. The Allan deviation analysis showed a factor of two increase in the uncertainty of



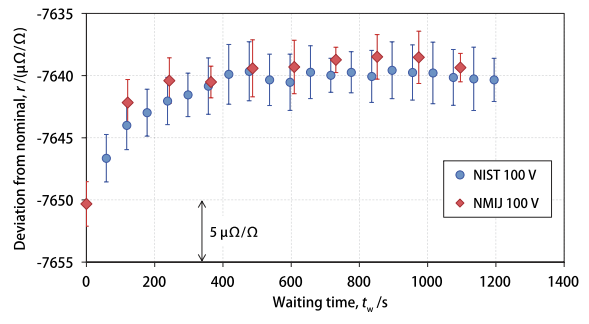
(a) 10 MΩ



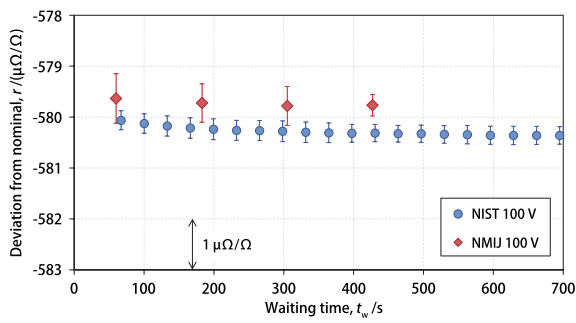
(e) 100 GΩ



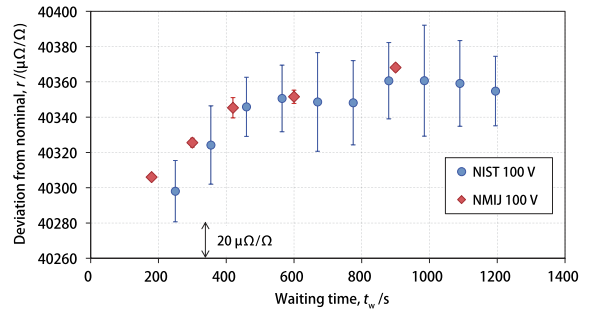
(b) 100 MΩ



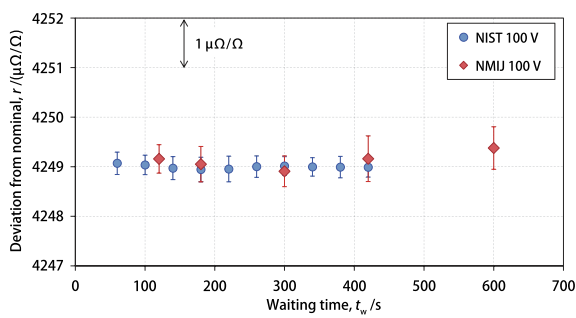
(f) 1 TΩ



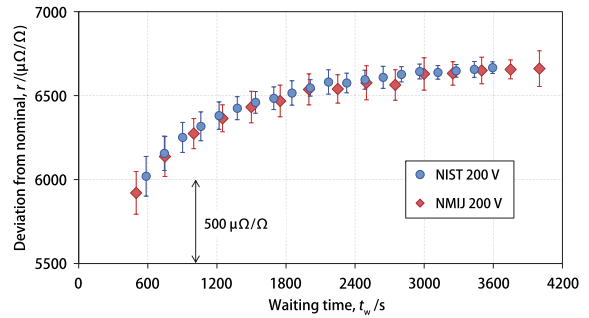
(c) 1 GΩ



(g) 10 TΩ



(d) 10 GΩ



(h) 100 TΩ

Figure 6. Settling time dependence of the resistors from 10 MΩ to 100 TΩ measured using the NMIJ traveling DSB and the NIST AWB.

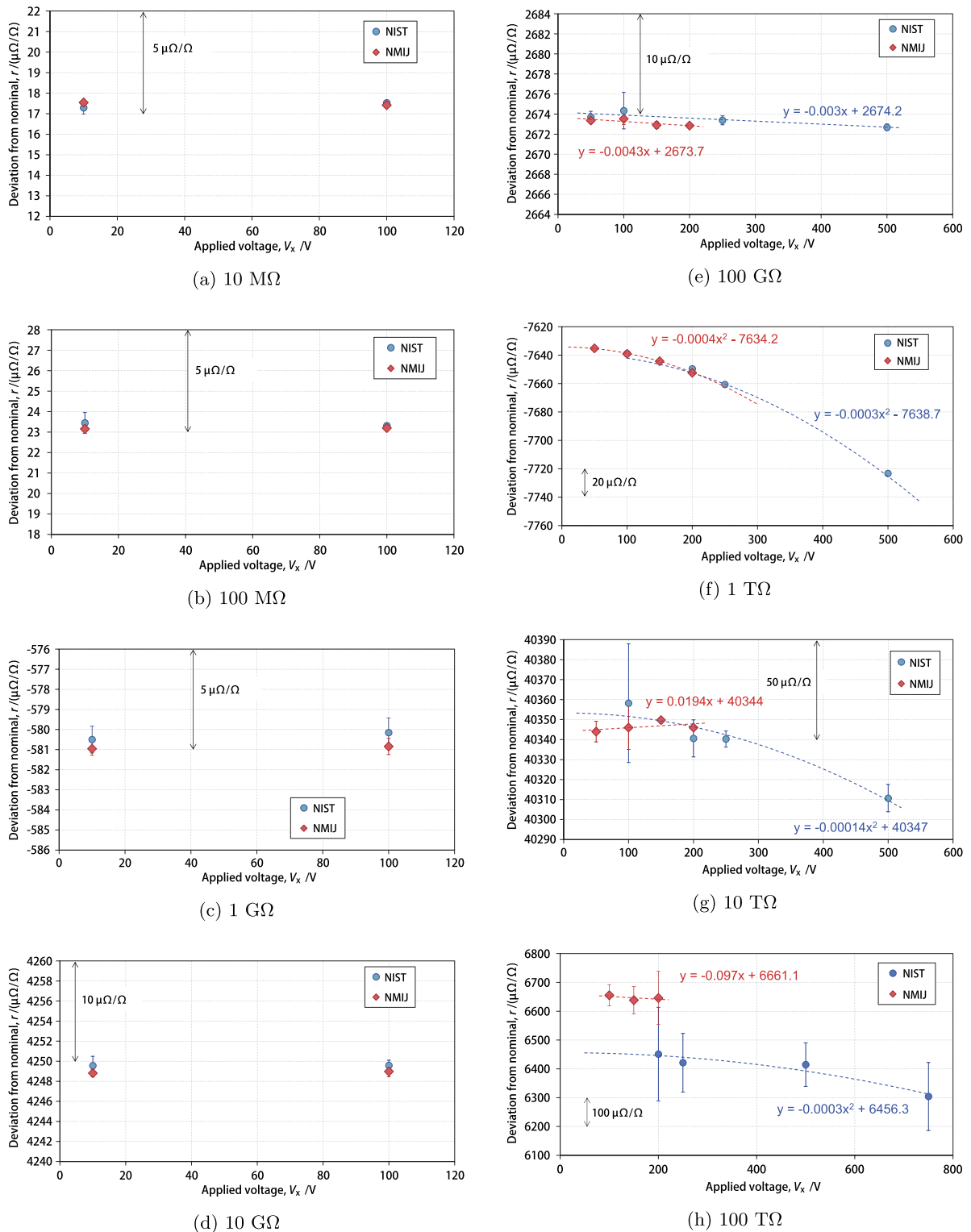


Figure 7. Voltage dependence of the resistors from 10 MΩ to 100 TΩ measured using the NMIJ traveling DSB and the NIST AWB.

the current resolution when auto range was used for resistance ranges of 1 TΩ and above. Resistance measurements in these ranges were made by selecting 1 pA rather than the auto range function to reduce the noise to get better current resolution.

4. Measurement results

At the beginning of the comparison, the settling time dependence was evaluated in both NMIJ and NIST systems. Figure 6

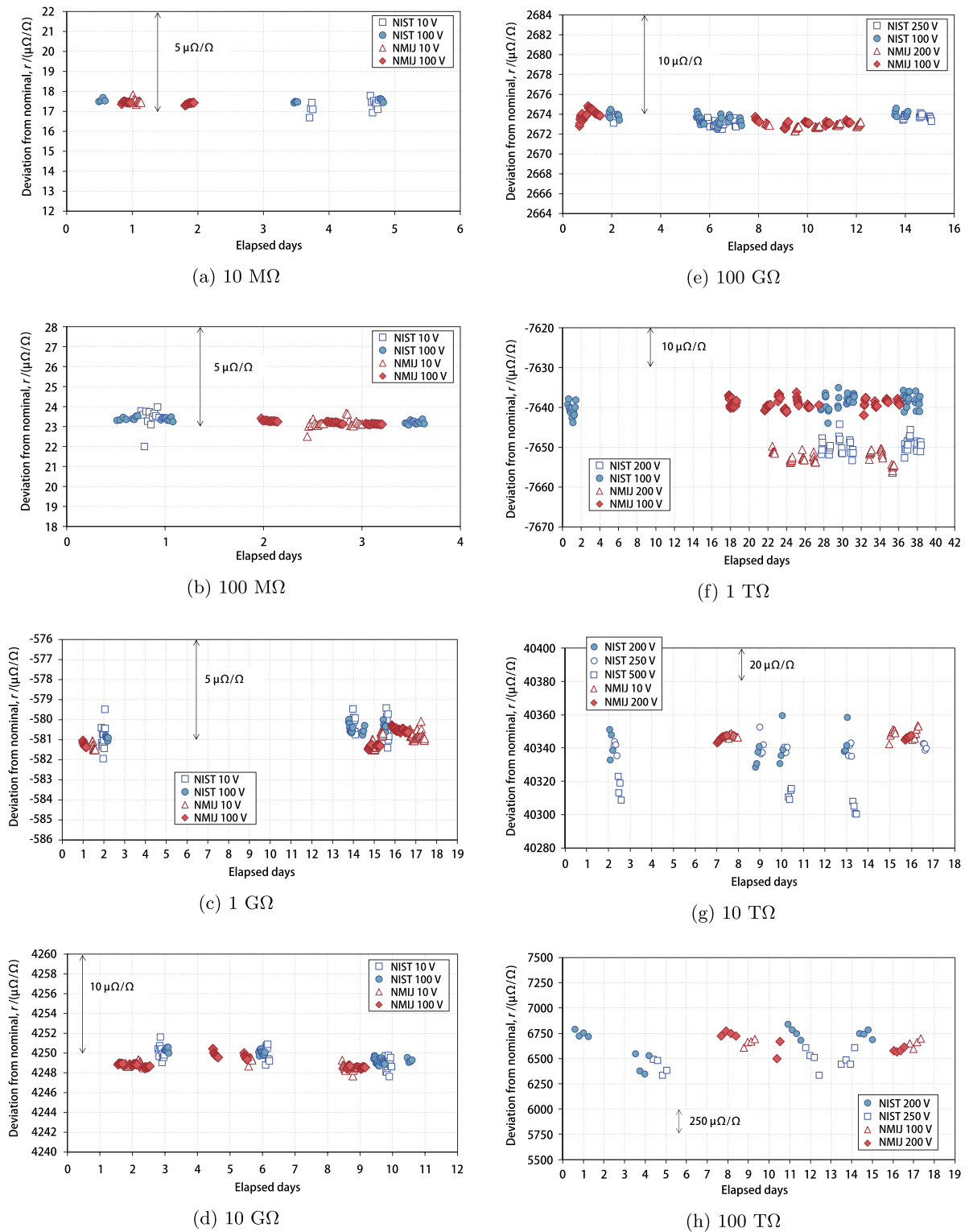


Figure 8. High resistance comparison results from 10 MΩ to 100 TΩ between the NMIJ traveling DSB and the NIST AWB.

shows the settling time dependence results from 10 MΩ to 100 TΩ. At the beginning of this evaluation, many measurements were performed with various settling times, but resulted in really long time to finish all measurements and was difficult to get repeatable results due to the drift of the resistance value over many weeks. Some results in figure 6 were taken this way but finally, the settling time dependence was calculated

from some long measurement results and all NIST results in the figure were taken this way. Although some results show some differences in the resistance value between the NIST and the NMIJ due to the different measurement dates, the difference was independent of the settling time for all standard resistors. The settling time is defined as the time from when the test voltages V_x and V_s were applied to the standard resistors

Table 3. High resistance comparison results from 10 MΩ to 100 TΩ between the NMIJ traveling DSB and the NIST AWB.

R_x	NMIJ traveling DSB $R_x \pm U/\mu\Omega \Omega^{-1}$	NIST AWB $R_x \pm U/\mu\Omega \Omega^{-1}$	R_x difference (NMIJ–NIST)/ $\mu\Omega \Omega^{-1}$	R_x/R_s difference (NMIJ–NIST)/ $\mu\Omega \Omega^{-1}$	DoE(NMIJ) $d_{NMIJ} \pm U(d_{NMIJ})/$ $\mu\Omega \Omega^{-1}$	DoE(NIST) $d_{NIST} \pm U(d_{NIST})/$ $\mu\Omega \Omega^{-1}$
10 MΩ	17.4 ± 0.9	17.5 ± 0.4	–0.11	–0.11	–0.1 ± 0.8	0.0 ± 0.2
100 MΩ	23.2 ± 1.2	23.3 ± 0.6	–0.11	0.00	–0.1 ± 1.1	0.0 ± 0.3
1 GΩ	–580.8 ± 1.5	–580.5 ± 0.8	–0.69	–0.58	–0.6 ± 1.4	0.1 ± 0.3
10 GΩ	4249.0 ± 1.8	4249.6 ± 0.9	–0.61	0.09	–0.5 ± 1.6	0.1 ± 0.4
100 GΩ	2673.5 ± 2.0	2674.3 ± 1.1	–0.82	–0.22	–0.6 ± 1.8	0.2 ± 0.5
1 TΩ	–7639.0 ± 6.2	–7638.9 ± 1.7	–0.12	0.7	–0.1 ± 6.0	0.0 ± 0.4
10 TΩ	40 346 ± 47	40 341 ± 6.5	5.4	5.5	5.3 ± 46	–1.0 ± 0.9
100 TΩ	6646 ± 468	6651 ± 101	–5.6	–11.0	–5.4 ± 458	0.2 ± 21

to when the current measurements are used to determine R_x . As shown in figure 6, both institutes results showed similar behavior with respect to the waiting time, implying that we can make comparisons at any common waiting time, but we made the comparisons with the waiting time long enough to settle the results. For example, over 400 s waiting time is adequate for the 1 TΩ and we chose the waiting time of 3600 s for the 100 TΩ comparison.

The voltage dependence of all resistances was evaluated with both systems as shown in figure 7. The NMIJ traveling DSB can make measurements with the voltages up to 200 V due to the allowable voltage of the latching relays for the voltage ratio measurement. High resistance elements usually do not show a clear correlation between the voltage dependence and the temperature coefficient as in low and intermediate resistance range, and it is difficult to say which is adequate, linear, or polynomial as the approximation curve. In this figure, an approximate expression that more closely matches the experimental results was adopted. In the 100 TΩ result, about 200 $\mu\Omega \Omega^{-1}$ difference was observed between NMIJ and NIST due to the resistance change, but we obtained similar voltage dependence results in all resistance ranges. From the results, the correction value against the applied voltage was determined in all resistance ranges for both systems individually, and different correction value was applied for the R_s value for each system to perform the comparison as correct as possible.

Figure 8 shows the measured results from 10 MΩ to 100 TΩ by the NMIJ traveling DSB and the NIST AWB. The horizontal axis shows the elapsed days from the measurement start date. All of the resistors were stable within the type A uncertainty of measurements during the whole measurement day and the measurement results by both NMIs were in good agreement within the dispersion. Table 3 summarises the measurement results and the degrees of equivalence (DoE) for each system. The second and third columns show the measurement result and the expanded uncertainty ($k = 2$), and fourth and fifth columns show the difference of R_x value and the measured resistance ratio, R_x/R_s , respectively. The same 1 MΩ value was used as the reference standard for the 10 MΩ measurement for both systems, and for the higher resistance measurements, each system used its own calibrated value for the reference resistor (R_s) for each step. Therefore the third column shows the accumulated difference

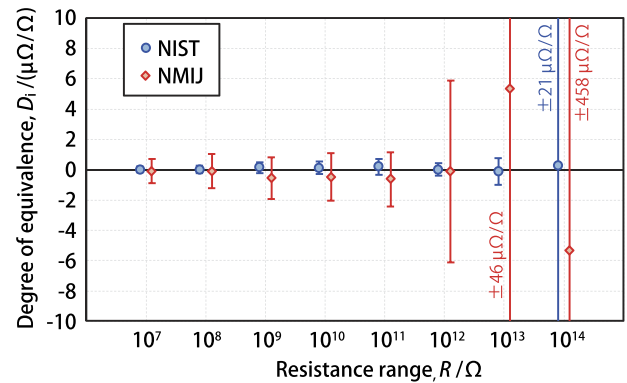


Figure 9. DoE for the measurements from 10 MΩ to 100 TΩ between NIST and NMIJ.

of the measured R_x value based on the same 1 MΩ value, and the fourth column shows the ratio difference at each resistance range. The measured values in table 3 were derived by taking the average of the measured values plotted with filled points in figure 8. 1 TΩ to 100 TΩ resistors showed bigger and clear voltage dependence as shown in figures 7 and 8(f)–(h), therefore the difference between NMIJ and NIST was calculated using the values measured using same applied voltage.

The right two columns of table 3 show the DoE with the reference value calculated from the weighted mean of both results [31] and the expanded uncertainties for each system. Figure 9 plots the DoE values, the deviation from the reference value, and the values were low enough in all resistance range and less than 6 $\mu\Omega \Omega^{-1}$ even at 10 TΩ and 100 TΩ.

5. Conclusion

A high resistance comparison between the NMIJ traveling DSB and the NIST AWB from 10 MΩ to 100 TΩ was performed at NIST. Generally, this comparison is performed using traveling standard resistors but the quality of the comparison result is completely limited by the stability of the traveling resistors. Therefore, in this comparison, the NMIJ traveling DSB system was shipped to the NIST Gaithersburg campus and was installed next to the NIST AWB system. Both systems adopt DSB configuration, but the NMIJ traveling system has an additional digital multimeter to measure the voltage ratio of the applied voltages during the measurement. Since the NMIJ measures the voltage ratio after get-

ting the bridge balance with some offsets for each polarity and for every measurement points, the measurement time is longer than the usual DSB configuration but the output voltage of the voltage sources do not need to be calibrated in advance. Moreover, it is expected that the linearity of the digital multimeter may be relatively more stable than the ratio of the two calibrated output voltages before and after the air transportation since the latter is the ratio of the output voltages of two independent instruments. Therefore a DSB with this configuration might be suitable as the traveling bridge.

To eliminate the influence of instabilities of the resistors including temperature coefficient and mechanical shock, the comparison was performed by measuring the resistors stored in the same temperature-controlled air bath, and we tried to not change the position of the resistors inside the air bath. The cables are also an important component for the precise measurement and we used dedicated cables for each system, however, this required opening the air bath to switch between the two measurement systems and a slight temperature change around the resistors might have occurred since the airflow inside the air bath might change by the position of the cables. Humidity coefficient was not considered since the humidity of the experimental room was well controlled and stable enough within the measurements time.

The comparison was performed by repeating 10 : 1 measurements from 10 M Ω to 100 T Ω based on the same 1 M Ω value calibrated by the NIST two-terminal CCC system to eliminate other deviation components and to compare the measurement capabilities of both systems. The calibrated resistance values up to 1 T Ω were determined from scaling by each system and agreed to within 1 $\mu\Omega \Omega^{-1}$, and the DoE values were less than 6 $\mu\Omega \Omega^{-1}$ in all resistance ranges for each system. These results show improved uncertainties over traveling resistor comparisons in the high resistance range, and in the future, the similar comparison between the NMIJ's voltage injection type Wheatstone bridge system that is used in Japan for the customer calibration and the traveling DSB system evaluated in this paper will be performed.

ORCID iDs

T Oe  <https://orcid.org/0000-0003-3424-1745>

S Payagala  <https://orcid.org/0000-0001-6359-8765>

A R Panna  <https://orcid.org/0000-0001-6557-2112>

S Takada  <https://orcid.org/0000-0002-7831-585X>

N-H Kaneko  <https://orcid.org/0000-0003-3857-7940>

D G Jarrett  <https://orcid.org/0000-0003-1392-423X>

References

- [1] Jarrett D G, Oe T, Kaneko N-H and Payagala S U 2018 10 T Ω and 100 T Ω resistance comparison between NIST and AIST *CPEM 2018 Conf. Digest*
- [2] Sanchez C and Wendler K 2020 Final report of the CCEM-K2.2012 key comparison of resistance standards at 10 M Ω and 1 G Ω *Metrologia* **57** 01006
- [3] Jeckelmann B et al 2013 Final report on supplementary comparison EURAMET.EM-S32: comparison of resistance standards at 1 T Ω and 100 T Ω *Metrologia* **50** 01008
- [4] Galliana F, Capra P P and Gasparotto E 2011 Evaluation of two alternative methods to calibrate ultrahigh value resistors at INRIM *IEEE Trans. Instrum. Meas.* **60** 965–70
- [5] Giem J I 1991 Sub-ppm linearity testing of a DMM using a Josephson junction array *IEEE Trans. Instrum. Meas.* **40** 329–32
- [6] Maruyama M, Takahashi H, Katayama K, Yonezawa T, Kanai T, Iwasa A, Urano C, Kiryu S and Kaneko N-H 2015 Evaluation of linearity characteristics in digital voltmeters using a PJVS system with a 10 K cooler *IEEE Trans. Instrum. Meas.* **64** 1613–19
- [7] van den Brom H E, Houtzager E, Rietveld G, van Bemmelen R and Chevchenko O 2007 Voltage linearity measurements using a binary Josephson system *Meas. Sci. Technol.* **18** 3316
- [8] Lee K C, Cage M E and Rowe P S 1994 Sources of uncertainty in a DVM-based measurement system for a quantized Hall resistance standard *J. Res. Natl Inst. Stand. Technol.* **99** 227–40
- [9] Dziuba R F, Jarrett D G, Scott L L and Secula A J 1999 Fabrication of high-value standard resistors *IEEE Trans. Instrum. Meas.* **48** 333–7
- [10] Payagala S U, Panna A R, Rigosi A F and Jarrett D G 2020 Advanced temperature-control chamber for resistance standards *J. Res. Natl Inst. Stand. Technol.* **125** 125012
- [11] Henderson L 1987 A new technique for the automatic measurement of high value resistors *J. Phys. E: Sci. Instrum.* **20** 492–5
- [12] Hernandez-Marquez F L, Bierzychudek M E, Jones G R Jr and Elmquist R E 2014 Precision high-value resistance scaling with a two-terminal cryogenic current comparator *Rev. Sci. Instrum.* **85** 044701
- [13] Elmquist R E, Hourdakis E, Jarrett D G and Zimmerman N M 2005 Direct resistance comparisons from the QHR to 100 M/spl Omega/using a cryogenic current comparator *IEEE Trans. Instrum. Meas.* **54** 525–8
- [14] Oe T, Payagala S U, Jarrett D G and Kaneko N H 2020 Evaluation of NMIJ traveling dual source bridge using NIST adapted Wheatstone bridge *CPEM 2020 Conf. Digest*
- [15] Oe T, Kinoshita J and Kaneko N-H 2012 Voltage injection type high ohm resistance bridge *CPEM 2012 Conf. Digest* pp 360–361
- [16] FEMTO Messtechnik GmbH 2016 Variable gain sub femto ampere current amplifier DDPCA-300 Datasheet
- [17] Finardi I and Callegaro L 2018 Calibration setup for ultralow-current transresistance amplifiers *IEEE Trans. Instrum. Meas.* **67** 2676–83
- [18] Rietveld G and van der Beek J H N 2013 Automated high-Ohmic resistance bridge with voltage and current null detection *IEEE Trans. Instrum. Meas.* **62** 1760–65
- [19] Jarrett D G and Elmquist R E 2004 Settling times of high-value standard resistors *CPEM 2004 Conf. Digest* (London, United Kingdom) pp 522–3
- [20] Schumacher B and Melcher J 2010 Automated high-value resistance calibration up to 1 P Ω *CPEM 2010 Conf. Digest* pp 635–6
- [21] Jarrett D G, Payagala S U, Kraft M E and Yu K M 2016 Third generation of adapted Wheatstone bridge for high resistance measurements at NIST *CPEM 2016 Conf. Digest*
- [22] Jarrett D G 1999 Evaluation of guarded high-resistance Hamon transfer standards *IEEE Trans. Instrum. Meas.* **48** 324–8
- [23] Jarrett D G and Kraft M E 2013 10 T Ω and 100 T Ω resistance measurements at NIST *X-Semetro Congress. Digest* (Buenos Aires, Argentina) pp 25–7
- [24] Hamon B V 1954 A 1–100 build-up resistor for the calibration of standard resistors *J. Sci. Instrum.* **31** 450–3

- [25] Cutkosky R D 1978 A new switching technique for binary resistive dividers *IEEE Trans. Instrum. Meas.* **27** 421–2
- [26] Tsao S H 1987 A 25 bit reference resistive voltage divider *IEEE Trans. Instrum. Meas.* **IM-36** 285–90
- [27] Sauer S H A 1968 Wye-delta transfer standards for calibration of wide range dc resistance and dc conductance bridges *IEEE Trans. Instrum. Meas.* **17** 151–5
- [28] Yu K M, Jarrett D G, Rigosi A F, Payagala S U and Kraft M E 2020 Comparison of multiple methods for obtaining $P\Omega$ resistances with low uncertainties *IEEE Trans. Instrum. Meas.* **69** 3729–38
- [29] Keysight Technologies 2019 Calculating uncertainty using digital multimeter ratio measurement techniques Application Note 5992–1058
- [30] Witt T J 2001 Using the Allan variance and power spectral density to characterize DC nanovoltmeters *IEEE Trans. Instrum. Meas.* **50** 445–8
- [31] Cox M G 2002 The evaluation of key comparison data *Metrologia* **39** 589–95